Published in final edited form as:
J Comp Neurol. 2014 June 1; 522(8): 1915–1928. doi:10.1002/cne.23511.

CORTICAL INPUTS INNERVATE CALBINDIN-IMMUNOREACTIVE INTERNEURONS OF THE RAT BASOLATERAL AMYGDALOID COMPLEX

Gunes Unal[1], **Jean-Francois Paré**[2], **Yoland Smith**[2], and **Denis Paré**[1,*]

[1]Center for Molecular & Behavioral Neuroscience, Rutgers University, Newark, NJ 07102

[2]Yerkes National Primate Research Center and Department of Neurology, Emory University, 954 Gatewood Road, Atlanta, GA 30329

Abstract

The present study was undertaken to shed light on the synaptic organization of the rat basolateral amygdala (BLA). The BLA contains multiple types of GABAergic interneurons that are differentially connected with extrinsic afferents and other BLA cells. Previously, it was reported that parvalbumin immunoreactive (PV^+) interneurons receive strong excitatory inputs from principal BLA cells but very few cortical inputs, implying a prevalent role in feedback inhibition. However, because prior physiological studies indicate that cortical afferents do trigger feedforward inhibition in principal cells, the present study aimed to determine whether a numerically important subtype of interneurons, expressing calbindin (CB^+), receives cortical inputs. Rats received injections of the anterograde tracer *Phaseolus vulgaris*-leucoagglutinin (PHAL) in the perirhinal cortex or adjacent temporal neocortex. Light and electron microscopic observations of the relations between cortical inputs and BLA neurons were performed in the lateral (LA) and basolateral (BL) nuclei. Irrespective of the injection site (perirhinal or temporal neocortex) and target nucleus (LA or BL), approximately 90% of cortical axon terminals formed asymmetric synapses with dendritic spines of principal BLA neurons, while 10% contacted the dendritic shafts of presumed interneurons, half of which were CB^+. Given the previously reported pattern of CB co-expression among GABAergic interneurons of the BLA, these results suggest that a subset of PV-immunonegative cells that express CB, most likely the somatostatin-positive interneurons, are important mediators of cortically-evoked feedforward inhibition in the BLA.

Keywords

amygdala; calbindin; feedforward inhibition; electron microscopy; tract-tracing

The amygdala plays a pivotal role in the acquisition, consolidation, and expression of emotional memories (Davis, 2000; LeDoux, 2000; McGaugh, 2000; Everitt et al., 2003). The basolateral complex of the amygdala (BLA), and particularly its lateral (LA) nucleus, is critical for these functions, because it constitutes the main entry point for sensory inputs from the thalamus and cortex into the amygdala (Russchen, 1986; LeDoux et al., 1990; Turner and Herkenham, 1991; McDonald, 1998). However, the neural networks and microcircuits that underlie the transmission and processing of this incoming information through the BLA remain unclear.

*Send correspondence to: Denis Paré Center for Molecular & Behavioral Neuroscience Rutgers, the State University of New Jersey 197 University Ave. Newark, NJ 07102, USA Tel: 973-353-3251 Fax: 973-353-1272 pare@andromeda.rutgers.edu.

CONFLICT OF INTEREST STATEMENT: The authors state that they have no conflict of interest.

As in the cerebral cortex, there are two main cell types in the BLA (reviewed in McDonald, 1992a). The main class of neurons (≈85%) consists of glutamatergic projection cells with highly collateralized axons and spiny dendrites. Their excitability is regulated by GABAergic local-circuit neurons that are aspiny or sparsely spiny, morphologically heterogeneous, and express various combinations of peptides such as cholecystokinin (CCK), somatostatin (SOM), vasoactive intestinal polypeptide (VIP), and calcium binding proteins (Kemppainen and Pitkänen, 2000; Katona et al., 2001; McDonald and Betette, 2001; Mascagni and McDonald, 2003; reviewed in Spampanato et al., 2011).

As in the cerebral cortex (Freund and Buzsaki, 1996; Markram et al., 2004; Blatow et al., 2005; Somogyi and Klausberger, 2005), different subtypes of BLA interneurons regulate the activity of principal cells in distinct ways because they target different postsynaptic domains (Muller et al., 2003, 2006, 2007; Bienvenu et al., 2012) and receive contrasting sets of inputs (Smith et al., 2000). For instance, parvalbumin-immunoreactive (PV^+) interneurons appear to be mainly involved in feedback inhibition: they receive strong excitatory inputs from BLA projection cells, but very few from the cerebral cortex (Smith et al., 2000) and they form numerous inhibitory synapses on the somatic, axonal, and proximal dendritic domains of projection neurons (Pitkänen and Amaral, 1993; Sorvari et al., 1995; Smith et al., 1998; Kemppainen and Pitkänen, 2000; McDonald and Betette, 2001; reviewed in Spampanato et al., 2011).

Other types of interneurons likely generate feedforward inhibition in the BLA. Indeed, thalamic or cortical stimuli evoke inhibitory postsynaptic potentials (IPSPs) in principal cells (Rainnie et al., 1991; Washburn and Moises, 1992b; Lang and Paré, 1997ab, 1998; Danober and Pape, 1998; Martina et al., 2001). These IPSPs likely result from the activation of local-circuit neurons because they are responsive to cortical stimuli (Lang and Paré, 1998; Mahanthy and Sah, 1998; Szinyei et al., 2000; Bauer and LeDoux, 2004). However, the identity of the interneurons generating cortically-evoked feedforward inhibition remains unclear. Therefore, the present study was undertaken to examine whether a numerically important sub-class of BLA interneurons expressing calbindin (CB^+) receives direct cortical inputs. To maximize the likelihood of detecting synaptic contacts between cortical afferents and CB^+ interneurons at the electron microscopic level, we focused on two cortical fields that contribute very strong inputs to the BLA (reviewed in McDonald, 1998): the perirhinal cortex (PRC) and the ventral associative temporal neocortex, hereafter abbreviated NC for simplicity.

MATERIALS AND METHODS

Tract-tracing

The surgical procedures were conducted in accordance with the NIH Guide for the Care and Use of Laboratory Animals and approved by the Institutional Animal Care and Use Committees of Rutgers and Emory Universities. A total of 26 adult male Sprague-Dawley rats weighing 220–320 g were used in this study. The animals were kept in a 12-hour light/dark cycle with *ad libitum* food and water. They were anesthetized with isoflurane and administered atropine (0.05 mg/kg, i.m.) to aid breathing. After placing the rats in a stereotaxic apparatus and shaving their scalp, we made numerous small injections of the analgesic bupivacaine (0.125% solution, s.c.) around the sites to be incised. Ten minutes later, under sterile conditions, the scalp was opened above the cortical regions of interest, small holes were drilled into the skull, and the *dura mater* was opened.

The rats then received unilateral injections of the anterograde tracer *Phaseolus vulgaris*-leucoagglutinin (PHAL, Vector Laboratories, Burlingame, CA) in the cortical regions of interest, as previously described (Unal et al., 2013). In order to obtain a sufficient number of

anterogradely labeled axon terminals for electron microscopic observations, we performed relatively large PHAL injections, which involved both superficial and deep cortical layers. PHAL (2.5%) was dissolved in 0.01M phosphate buffer (PB; pH 8.0) and injected iontophoretically through a glass pipette (tip diameter: 25–30 μm) using positive 7 μA current pulses (7 sec on / 7 sec off) for 15 min. PRC injections targeted both areas 36 and 35 and were performed either rostrally (at the level of the amygdala) or caudally (at the level of the mesencephalo-diencephalic junction). Similarly, NC injections were either performed rostrally, in the ventral portion of the secondary auditory cortex, or caudally, in the temporal association cortex (Paxinos and Watson, 2007). However, the synaptic interactions between cortical axon terminals and BLA neurons did not vary with the anteroposterior level of the PHAL injection sites. Therefore, the result obtained following rostral and caudal PHAL injections are pooled in the results section. The stereotaxic coordinates (in mm relative to bregma for AP and ML, and from the dura mater for DV) were: rostral PRC (AP, −3.3; ML, 6.3; DV, −4.6), caudal PRC (AP, −5.2; ML, 7.1; DV, −4.1), rostral NC (AP, −3.3; ML, 6.3; DV, −3.2), and caudal NC (AP, −5.2; ML, 7.1; DV, −3.1). These coordinates were determined using a stereotaxic atlas of the rat brain (Paxinos and Watson, 2007).

After a survival period of 10–12 days, the animals were deeply anesthetized with sodium pentobarbital (50 mg/kg, i.p.) and perfused through the heart with 50–100 ml of 0.9% saline, followed by 500 ml of a fixative containing 0.1% glutaraldehyde and 4% depolymerized paraformaldehyde in 0.1M PB (pH 7.4). The brains were then removed, cut into blocks containing the regions of interest, and post-fixed in the same fixative overnight. The tissue blocks were then sectioned at 60 μm using a vibrating microtome and collected in PBS (0.1 M; pH 7.4).

Immunohistochemistry

Overview of methods and specificity of antibodies—For light and electron microscopy (EM), PHAL was detected with the immunoperoxidase method, using diaminobenzidine (DAB) as a chromogen. CB immunohistochemistry for light microscopic observations relied on the immunoperoxidase method, using nickel-intensified DAB as a chromogen, while the pre-embedding immunogold-silver intensification procedure was used to detect CB labeling at the EM level.

We used a rabbit anti-PHAL (1:1000, Vector Labs, Burlingame, CA) antibody. It should be noted that no differentiated labeling was seen when the PHAL antibody was used on brain sections obtained from animals that did not receive PHAL injections. For CB, we used a mouse monoclonal anti-calbindin-D-28K antibody (Sigma-Aldrich, St. Louis, MO; catalog # C9848) derived from the CB-955 hybridoma that was produced by fusing mouse myeloma cells with splenocytes of BALB/c mice immunized with purified bovine kidney calbindin-D-28K. Western blotting revealed positive signals in cultured hippocampal neurons from rat (Chard et al., 1995) and enterochromaffin cells of the human appendix (Katsetos et al., 1994), both detected as a band with a molecular weight of 28kDa. It was tested for specificity with western blotting by Sigma-Aldrich and found not to react with other calcium-binding proteins in the EF-hand family, such as calretinin and parvalbumin.

Immunohistochemistry for light microscopic observations—For light microscopic observations of PHAL labeling, we incubated the sections in sodium borohydride (1% in PBS) for 20 min at room temperature. They were then rinsed repeatedly in phosphate-buffered saline (PBS; 0.01M, pH 7.4) and incubated for 60 min in a PBS-based blocking solution that contained 1% bovine serum albumin (BSA), 1% normal goat serum (NGS), and 0.03% Triton X-100. Next, the sections were incubated overnight in the rabbit anti-PHAL antibody (1:1000, Vector Labs, Burlingame, CA). The next day, they were

rinsed in PBS (3 × 10 min), incubated for 90 min in biotinylated goat anti-rabbit IgG (1:200, Vector Laboratories, Burlingame, CA), and rinsed again in PBS (3 × 10 min). The sections were then incubated in the avidin-biotin peroxidase complex (ABC, Vector Labs, Burlingame, CA) for 90 min. A Tris-buffered saline (TBS) solution containing 0.025% DAB and 0.006% hydrogen peroxide was used to reveal the peroxidase for 10 min, which was followed by several rinses in 0.01 M PBS (pH 7.4). Finally, the sections were mounted onto glass slides, air-dried, dehydrated in a graded series of alcohol, and coverslipped in Permount mounting medium (Fisher Scientific, Pittsburgh, PA) for light microscopic observations.

In order to visualize PHAL- and CB-immunoreactive profiles in the same sections at the light microscopic level, we used a two-color dual-labeling immunoperoxidase technique (Hancock, 1986). After pre-incubation with the above blocking solution, the sections were incubated overnight in a solution containing both, the PHAL and CB antibodies. The next day, we first revealed PHAL exactly as described above. Once the PHAL was revealed, the sections were rinsed thoroughly and incubated in biotinylated horse anti-mouse IgG (1:200, Vector Laboratories, Burlingame, CA) for 90 min. Then, they were rinsed in PBS (3 × 10 min) and incubated for 90 min in ABC (1:100, Vector Labs, Burlingame, CA). Finally, the sections were washed twice in PBS and placed in a TBS solution containing 0.025% DAB, 0.37% nickel-intensified DAB chromogen (Ni-DAB) and 0.0012% hydrogen peroxide for about 5 minutes, until the black reaction product was strong enough without overshadowing the PHAL (brown).

Immunohistochemical procedures for EM observations—PHAL and CB immunoreactivity were revealed in the same sections. The sections were first incubated in sodium borohydride (1% in PBS) for 20 min at room temperature, followed by repeated rinses with PBS. Then, the sections were transferred to a cryoprotectant solution (25% sucrose and 10% glycerol in PB, 0.05 M, pH 7.4) for 20 min and placed in a −80°C freezer for an additional 20 min to permeabilize cell membranes. The sections were then thawed at room temperature and incubated in decreasing concentrations of the cryoprotectant solution, followed by incubation in a PBS solution containing 5% milk for 30 min and multiple rinses in TBS-gelatin (pH 7.6; 3 × 5 min). For incubation with the primary antibodies, the sections were transferred to a TBS-gelatin solution containing 1% milk, and a cocktail of mouse anti-calbindin-D-28K antibody (1:4000, Sigma-Aldrich, St. Louis, MO) and rabbit anti-PHAL antibody (1:1000, Vector Labs, Burlingame, CA) for 24 hours. Next day, the sections were rinsed in TBS-gelatin (3 × 10 min) and incubated for 2 hours in a TBS-gelatin solution containing 1% milk and the secondary antibodies: gold-conjugated goat anti-mouse IgGs (1:100, Nanogold, Nanoprobes, Stonybrook, NY) and biotinylated goat anti-rabbit IgGs (1:200, Vector Laboratories, Burlingame, CA). The sections were then rinsed with TBS-gelatin (2 × 10 min) and an aqueous acetate buffer solution (2%; pH 7.0) for 10 min. The HQ silver kit (Nanoprobes, Stonybrook, NY) was used in a dark room for silver intensification of gold particles for 10 min. Following silver intensification, the sections were rinsed repeatedly in acetate buffer and transferred to TBS-gelatin for 10 min. They were then incubated with the ABC solution in TBS-gelatin with 1% milk for 90 min, rinsed in TBS-gelatin (2 × 10 min) and TBS (10 min). Finally, the sections were incubated in DAB (0.025%) for 10 min at room temperature and rinsed thoroughly in PBS. At the end of the incubations, the sections were transferred in 0.1M PB (pH 7.4) for 5 min, rinsed several times in PB and postfixed in osmium tetroxide (0.5% in PB) for 10 min. After having been washed several times in PB, sections were dehydrated in a graded series of alcohol and propylene oxide. In order to improve contrast in the electron microscope, the sections were incubated in a 70% alcohol solution with 1% uranyl acetate for 10 minutes. Following dehydration, the sections were embedded in Durcupan resin (Fluka, Gymea, Australia), transferred to glass slides, coverslipped, and left in the oven at 60°C for 48 hours for

polymerization. BLA regions of interest were cut and removed from the glass, embedded onto resin blocks and trimmed in trapezoidal shape. The blocks were then sectioned at 70 nm with a 45°-diamond knife using an ultramicrotome (Ultracut-T, Leica Microsystems, Wetzlar, Germany). Ultrathin sections were collected onto single slot copper grids. Last, the grids were counterstained with Reynold's lead citrate, air-dried, and stored in grid boxes for electron microscopic observations.

We first examined the slides prepared for light microscopy in order to determine the location of the PHAL injection sites in each animal. We only considered cases where the injection sites were restricted to the targeted locations (PRC or NC) and led to robust anterograde labeling in the BLA. In all selected cases, the PHAL-labeled axons overlapped with CB-immunoreactive elements in the BLA. For electron microscopic analysis, we examined two to six blocks of tissue from each of the selected cases. Only the most superficial ultrathin sections of the blocks were considered to ensure optimal penetration of the antibodies. Grids were examined in a transmission electron microscope (80 kV; magnification 10,000 to 60,000; JEM-1011, JEOL, Peabody, MA) and micrographs were digitally imaged by an 11 Megapixel lens-coupled CCD camera (ES1000W, Gatan, Warrendale, PA).

Data analysis

In the EM, PHAL-labeled terminals were readily identifiable by the presence of the electron-dense amorphous DAB reaction product, while CB immunoreactivity was assessed by the presence of silver-intensified gold particles. An element of interest was considered CB-immunoreactive (CB^+) when the concentration of gold particles in its confines was ≥ three times higher than in the whole micrograph. This was calculated by counting all the gold particles in the micrograph and dividing this number by the micrograph's total area.

We used previously established ultrastructural criteria to identify organelles, synaptic junctions, and other structures in the electron microscope (see Colonnier, 1981; Peters et al., 1991; DeFelipe and Fariñas, 1992). Dendritic spines could be readily identified as such when they were seen to emerge from the parent dendrite. When the spine and parent dendrite were not located in the same plane, spines were identified by the presence of a spine apparatus, as well as the lack of microtubules and mitochondria. In contrast, dendritic shafts were generally larger and included microtubules, mitochondria, endoplasmic reticulum, or a combination of these structures. Multivesicular bodies appeared as distinct clusters of spherical and/or ellipsoidal vesicles. Established morphological criteria were used to identify cell junctions and synapses. Chemical synapses were identified by the presence of a synaptic cleft, characteristic synaptic densities and accumulation of synaptic vesicles near the active zone in the presynaptic element. Gap junctions were identified by the apposition of the plasma membranes of two adjacent neurons forming a uniform intercellular gap (≤4nm; Peters et al., 1991; Peters and Palay, 1996).

In each animal, we identified a total of 100 PHAL-labeled ($PHAL^+$) terminals forming synapses: half in LA and half in BL. These $PHAL^+$ synapses were categorized based on the identity of the postsynaptic elements, which could be a CB-immunonegative (CB^-) dendrite, CB^-dendritic spine, or CB^+ dendrite. No CB^+ spines were observed.

Electron micrographs were captured by a CCD camera controlled by the DigitalMicrograph software (Gatan, Warrendale, PA). Photomicrographs were cropped into Adobe Photoshop CS5 (Adobe Systems Incorporated, San Jose, CA). Brightness and contrast adjustments were performed with the same software to insure uniformity in multi-panel figures. However, such adjustments were applied to the entire image. The photographs were then imported in Adobe Illustrator CS5 to add labels and scale bars. To evaluate the statistical

significance of differences in the incidence of pre- or post-synaptic elements, we used chi-square tests.

RESULTS

Light microscopic observations

We performed PHAL injections in cortical areas that strongly project to the BLA (Russchen, 1982; Witter and Groenewegen, 1986; Smith and Pare, 1994, Shi and Cassell, 1997, 1999), namely perirhinal areas 35 and 36 (hereafter termed PRC injections), as well as in secondary auditory cortex and the temporal association cortex (hereafter termed NC injections). Of the 26 animals with PRC (n=13) or NC (n=13) PHAL injections, six were selected for in depth analysis because the PHAL injection sites were confined to the regions of interest (PRC, n=3; NC, n=3) and they produced strong anterograde labeling of cortical axons in the BLA. Figure 1 shows representative examples of these PHAL injection sites at low (Fig. 1A, PRC; Fig. 1C, NC) and high magnifications (Fig. 1B, PRC; Fig. 1D, NC). The location of PHAL injection sites was identified by the presence of $PHAL^+$ somata (arrows in Fig. 1B, D).

Consistent with prior findings in cats (Russchen, 1982; Witter and Groenewegen, 1986; Smith and Pare, 1994) and rats (Shi and Cassell, 1997, 1999), the density of $PHAL^+$ axons was clearly higher in LA than BL following both PRC and NC injections. This can be seen in figure 2, which shows anterogradely labeled axons in the BLA at low (Fig. 2A, PRC; Fig. 2C, NC) and high magnifications (Fig. 2B, PRC; Fig. 2D, NC). Nevertheless, $PHAL^+$ PRC and NC axons could be seen to contribute numerous axonal varicosities in both LA and BL (white arrows in Fig. 2B, D).

To examine the spatial relationship between cortical axons and CB^+ interneurons of the BLA in the light microscope, we used a two-color immunoperoxidase method where PHAL and CB were revealed with the chromogens DAB and nickel-DAB, respectively (Fig. 3). As a result, anterogradely labeled cortical axons appeared brown whereas CB^+ elements were dark blue, making them easily distinguishable from each other in the light microscope. The distribution of CB^+ neurons in LA and BL was quite homogeneous. CB immunoreactivity labeled them in a Golgi-like manner, allowing an apparently complete visualization of their somata as well as their proximal and distal dendrites (Fig. 3A–E). Consistent with the notion that CB is almost exclusively expressed by local-circuit cells (McDonald and Mascagni, 2001), virtually all CB^+ dendrites examined were devoid of spines.

Following both, PHAL injections in the PRC or NC, profuse plexuses of anterogradely labeled cortical varicose axons and CB^+ processes were intermingled in the BLA (Fig. 3A and C, respectively). At a high magnification, numerous cases of close appositions between $PHAL^+$ axonal varicosities and CB^+ processes were observed (Fig. 3B,D). CB^+ processes in close apposition with $PHAL^+$ axonal varicosities included proximal (Fig. 3B, arrowheads) and distal (Fig. 3B, arrows) dendrites, but far less frequently, somata (Fig 3C, arrowhead). In many instances, the same $PHAL^+$ axon was seen to contribute multiple axonal varicosities in close apposition with dendrites belonging to different CB^+ neurons (Fig. 3D). Conversely, some CB^+ dendrites were often seen in close apposition with axonal varicosities contributed by different $PHAL^+$ axonal branches. As mentioned above, both PRC and NC injections led to significantly denser labeling in LA than BL, resulting in more areas of overlap between $PHAL^+$ and CB^+ elements in the former nucleus. This point is illustrated in figure 3C, which depicts the LA-BL border (dashed line). Note denser PHAL labeling in the upper part of the micrograph, corresponding to LA.

Electron microscopic observations

Although the light microscopic observations described above suggest that CB^+ interneurons of the BLA receive cortical inputs, EM observations are required to establish the existence of such synaptic interactions. Therefore, to determine whether cortical terminals and CB^+ interneurons are synaptically connected, sections of the amygdala were prepared for EM observations. In this material, PHAL immunoreactivity was revealed with the electron-dense amorphous DAB reaction product, whereas CB^+ processes were localized with silver-intensified immunogold particles.

Specificity of calbindin immunocytochemistry and ultrastructural features of CB^+ neurons—As shown in figure 4, the pre-embedding CB immunogold reaction led to a very low level of background labeling. Silver-intensified gold particles usually occurred as dense clusters within the confines of individual profiles, most often dendrites (Fig. 4), but also occasionally axons, or cell bodies. In contrast, adjacent non-immunoreactive dendritic profiles or spine heads in the same ultrathin section were usually devoid of gold particles. Below, a given element was considered CB^+ when the concentration of gold particles in its confines was at least three times higher than in the entire micrograph (see details in Methods). However, in most cases, the distribution of gold particles within different profiles present in the same section was so differentiated that no such calculation was required.

The following description is based on EM observations of 32 ultrathin sections obtained from six animals. CB^+ somata and dendritic profiles were abundant in both LA and BL. Consistent with our light microscopic observations, virtually all (>99%) CB^+ dendritic profiles we observed (n=324) lacked dendritic spines. The rare instances of CB^+ spiny dendrites could belong to the very small population of weakly CB-immunoreactive principal cells described previously (McDonald and Mascagni, 2001). In addition, we observed puncta adhaerentia between pairs of apposed dendritic profiles that were either both CB^+ (arrowheads in Fig. 5A, 3 of 12) or both CB^- (arrowhead in Fig. 5B, 4 of 21). In contrast, such interactions were not found between adjacent CB^+ and CB^- dendrites (n=15). Another ultrastructural property of CB^+ (24 of 326) and CB^- (37 of 413) dendritic profiles was the presence of intracellular multi-vesicular bodies that appeared as large (300 to 480 nm in diameter) membrane-delimited clusters of round to elliptical vesicles in the core of dendritic profiles. Examples of multivesicular bodies (endosomal organelles thought to be involved in molecular sorting and degradation; Hanson and Cashikaer, 2012) within CB^+ and CB^- dendritic profiles are shown in figures 4D and 5C,D respectively

Because earlier studies reported the presence of gap junctions between PV-expressing interneurons of the BLA (Muller et al., 2005; Woodruff and Sah, 2007), we scrutinized our material for evidence of electrical synapses that involved CB^+ elements in LA or BL. Although no instance of gap junctions involving CB^+ elements was seen in either nucleus, an example of such interactions was found between CB^- elements (arrows in Fig. 5B). Given that almost all CB^+ cells co-express PV in LA (McDonald and Mascagni, 2001), these electrically coupled cells likely belong to a different subgroup of interneurons, not expressing PV or CB.

Finally, we observed that some of the CB^+ dendritic shafts (n=3) that formed asymmetric synapses with $PHAL^+$ axon terminals, contained vesicular profiles (arrows in figure 7C,D). However, because these dendritic vesicles were neither located close to the plasma membrane or associated with chemical synapses, their functional significance remains unknown. Examination of serial ultrathin sections will be required to establish whether these vesicular dendritic profiles are associated with synaptic membrane specializations. Such an arrangement would suggest that CB^+ cells not only form inhibitory synapses via their axons, but also their dendrites.

Although dendrodendritic adherent junctions (Fig. 5A), multi-vesicular bodies, (Fig. 5C, D), and vesicular profiles (Fig. 7C,D), were not restricted to CB^+ elements, they were never observed in spiny dendrites, suggesting that they represent distinguishing ultrastructural features of BLA interneurons.

Synaptic interactions between cortical inputs and CB^+ interneurons of the BLA—For each of the six rats with PHAL injections confined to the PRC or NC, we analyzed the synaptic connections of 50 $PHAL^+$ axon terminals in LA and 50 in BL, for a total of 100 synapses per animal. Whenever possible, all 50 terminals were analyzed from the same grid. However, particularly for BL, several grids were required because the density of $PHAL^+$ terminal boutons was comparatively low. Note that to ensure proper penetration of the antibodies, we only considered superficial ultrathin sections with differentiated CB^+ labeling. Using this approach, we analyzed a total 600 $PHAL^+$ axon terminals forming synaptic contacts with either CB^+ or CB^- elements of the BLA. All of these synapses were asymmetric. Figure 6 provides frequency distributions of the elements postsynaptic to these $PHAL^+$ terminals. Figure 7 shows representative examples of these synapses.

Irrespective of the injection site (PRC or NC), nucleus observed (LA or BL), and in each animal, the vast majority of $PHAL^+$ terminals (≥88%) formed asymmetric axospinous synapses (Fig. 6). An example of such an axospinous synapse is illustrated in figure 7A. On average, 90.7% of $PHAL^+$ perirhinal and 91% of neocortical axon terminals formed axospinous synapses. All these spines were CB^- and presumed to belong to principal cells. Perirhinal and neocortical inputs did not differ in this respect (χ^2-test, $P = 0.99$) nor did the targeted region (LA vs. BL, χ^2-test, $P = 0.99$).

The remainder of the $PHAL^+$ axon terminals formed asymmetric synapses with dendritic profiles. Here again, this finding was consistent for the two injection sites (PRC, 9.3%; NC, 9%; χ^2-test, $P = 0.9$) and target nuclei (LA, 4.8% or BL, 4.4%; χ^2-test, $P = 0.83$). These dendritic profiles were divided roughly equally between CB^+ (PRC, 4.6%; NC, 4.7%) and CB^- (PRC, 4.7%; NC, 4.3%) elements (χ^2-tests; PRC, $P = 0.98$; NC, $P = 0.93$). Figure 7B shows an example of an axodendritic synapse between a $PHAL^+$ axon terminal and a CB^- element. Examples of $PHAL^+$ axon terminals contacting CB^+ dendritic profiles (28 of 55 axodendritic contacts) are depicted in figure 7C,D. Finally, it should be noted that the pattern of results described above did not vary whether the PHAL injections were performed at rostral vs. caudal PRC or NC levels.

DISCUSSION

While it is generally agreed that the BLA is critically involved in various aspects of memory formation, the underlying mechanisms remain unclear because our understanding of its intrinsic network is limited. Prior studies have revealed that the BLA contains multiple subtypes of GABAergic interneurons (reviewed in Spampanato et al., 2011). Based on similarities between the organization of the BLA and the cerebral cortex, these different types of local-circuit neurons are thought to regulate the activity of principal cells in distinct ways, but limited data is available on their connectivity. The present study addressed this gap in our knowledge by focusing on the connectivity of a numerically important subclass of BLA interneurons, expressing CB. To this end, we combined anterograde tracing of cortical inputs and CB immunocytochemistry. This approach revealed that approximately half the cortical inputs to local-circuit cells of the BLA target CB^+ interneurons. Therefore, our results suggest that CB interneurons constitute a major source of feedforward inhibition and a potential site of regulation for the induction of activity-dependent plasticity in principal cells of the BLA. Below, we consider the significance of these findings in light of prior anatomical and physiological studies on synaptic inhibition in the BLA.

Synaptic organization of the BLA

The cytoarchitecture and synaptic organization of the BLA is similar to that of the cerebral cortex in many ways. As in the cerebral cortex, principal cells are glutamatergic neurons with densely spiny dendrites whereas interneurons are mostly devoid of dendritic spines and use GABA as a transmitter (reviewed in Pape and Pare, 2010). As a result, it is commonly believed that, as in the cerebral cortex (Colonnier, 1981; Peters et al., 1991; DeFelipe and Fariñas, 1992), excitatory inputs to principal BLA cells form asymmetric synapses with dendritic spines. In contrast, asymmetric synapses on dendritic shafts are thought to represent excitatory inputs to BLA interneurons (Carlsen and Heimer, 1988; LeDoux et al., 1991; Smith and Pare, 1994; Pare et al., 1995; McDonald et al., 2002; Muller et al., 2003, 2006, 2007). In several studies, the identity of the pre- and/or postsynaptic elements involved in these axospinous and axodendritic synapses were identified using pre- or post-embedding immunocytochemistry for glutamate, GABA, or CAMKIIα, a marker of glutamatergic BLA neurons (for instance, see Smith and Pare, 1994; McDonald et al., 2002; Muller et al., 2007). Without exception, these studies supported the view that, in the BLA, asymmetric axospinous and axodendritic synapses largely represent glutamatergic inputs to principal cells vs. local-circuit neurons, respectively.

In the present study, we observed that around 90% of cortical axon terminals formed asymmetric synapses with dendritic spines presumed to belong to principal BLA cells, while approximately 10% of them contacted the dendritic shafts of putative interneurons. This pattern of synaptic connectivity was seen after both, perirhinal and temporal neocortical PHAL injections, and in the two target BLA nuclei examined (LA and BL). While the low proportion of axodendritic synapses might be construed as evidence that cortical inputs to interneurons are not potent drivers of inhibition, it is misleading. Indeed, projection cells account for about 85% of BLA neurons and their dendritic trees are much more extensive than that of most interneurons (McDonald, 1992; Lang and Pare, 1998). Thus, by chance alone, one would expect that only a minority of synapses formed by an extrinsic contingent of axons would contact local-circuit cells. In addition, other factors suggest that the synapses formed by cortical axons with BLA interneurons, even if low in number, can efficiently fire interneurons and lead to a potent inhibition of principal cells. Among them are the findings that, relative to principal cells, several interneuron subtypes have a higher input resistance, more depolarized resting potential, higher intrinsic excitability, and less negative GABA-A reversal potential (Lang and Pare, 1998; Mahanty and Sah, 1998; Martina et al., 2001; Rainnie et al., 2006; Woodruff and Sah, 2007; Sosulina et al., 2010). As a result, it is likely that comparatively fewer glutamatergic synapses are needed to fire local-circuit cells than projection neurons. In turn, interneurons generate strong IPSPs in principal cells via GABA-A and B receptors (Rainnie et al., 1991; Washburn and Moises, 1992b; Land and Paré, 1997ab, 1998; Danober and Pape, 1998; Martina et al., 2001). Therefore, it is likely that the cortical inputs on CB^+ cells identified in this study have a strong influence on the processing of incoming information by the BLA.

Identity of the BLA interneurons targeted by cortical inputs

Prior studies by McDonald and colleagues (McDonald and Betette, 2001; McDonald and Mascagni, 2001a, 2002; Mascagni and McDonald, 2003; Mascagni and McDonald, 2007) have revealed that the rodent BLA contains at least five types of GABAergic interneurons. In decreasing order of numerical importance, they are: (1) PV^+ cells (accounting for 20–40% of the GABAergic cells), (2) SOM^+ cells (representing 15% of GABAergic cells), (3) small cells expressing VIP plus CCK, (4) large multiploar CCK^+ cells and (5) cells expressing 5-HT-3A receptors, only a minority of which express other interneuronal markers. The same authors further reported that CB is often coexpressed by three of these five interneuron subtypes (PV^+, SOM^+, large CCK^+ cells). However, co-localization is

particularly prevalent among PV^+ and SOM^+ cells where as many as 80% of PV^+ and 90% of SOM^+ cells are also CB^+ (McDonald and Mascagni, 2001, 2002; Mascagni and McDonald, 2003).

At the moment, little data is available on the cortical afferents to these various types of GABAergic interneurons. To the best of our knowledge, only one study addressed this question in the BLA and it focused on PV^+ interneurons (Smith et al., 2000). Figure 8 compares the results obtained here (left) with those obtained in this prior study (right). This figure shows that cortical axon terminals form a much lower proportion of synapses with PV^+ than CB^+ interneurons. In contrast, the same study (Smith et al., 2000) reported that around 11% of terminals formed by the intranuclear axon collaterals of principal BLA neurons contact PV^+ cells.

Together, these findings therefore suggest that PV^+ cells are mainly involved in feedback inhibition, and that one or more subtype(s) of CB^+ cells, not expressing PV, are important targets of cortical inputs. However, an important caveat should be mentioned. The prior study on the cortical innervation of PV^+ interneurons (Smith et al., 2000) was not performed in rats but in cats and monkeys. Moreover, the cortical inputs examined in this prior study partially differed from those examined here (cats: perirhinal, entorhinal, pre/infralimbic cortices; monkeys: orbitofrontal region). Because different species and partially different sets of cortical areas were studied in the Smith et al. (2000) study and the present one, a comparison between the two studies, while suggestive, does not preclude the possibility that distinct cortical regions are differentially connected to the same interneuronal populations or that species differences exist in the termination pattern of the same inputs. Although these possibilities cannot be excluded at this time, in our opinion they are unlikely because the organization of the amygdala's GABAergic system in general (McDonald and Pearson, 1989; McDonald and Augustine, 1993; Pare and Smith 1993), and of PV^+ cells in particular appears similar in rats, cats, and monkeys (Pitkanen and Amaral, 1993; Smith et al., 1998; McDonald and Mascagni, 2001). For instance, as seen in rats where PV^+ cells account about for respectively 43% vs. 19% of GABAergic cells in BL and LA (McDonald and Mascagni, 2001), in cats there are more PV cells in BL than LA, with some parts of LA being nearly devoid of PV^+ cells (Smith et al., 1998). Nevertheless, in the present study, we found that cortical inputs to CB^+ cells were as numerous in BL and LA.

Therefore, the following account assumes that there are no species differences in the cortical innervation of distinct interneuronal populations. The findings of the Smith et al. (2000) study combined with the present ones suggest that one or more subtype(s) of CB^+ cells, not e last expressing PV, are important targets of cortical inputs. Given the previously reported pattern of CB co-expression (McDonald and Mascagni, 2001, 2002; Mascagni and McDonald, 2003), these results suggest that a subset of PV^- cells expressing CB, most likely the SOM^+ or large CCK^+ cells are important mediators of cortically-evoked feedforward inhibition in the BLA. Because SOM^+ cells constitute a sizable proportion of BLA interneurons (15%; McDonald and Mascagni, 2002), they represent the most likely possibility. These interneurons are interesting because they prevalently target the distal dendrites of principal cells (Muller et al., 2007). In addition, a proportion of their axon terminals form inhibitory synapses with other interneurons, mainly the PV^+ and VIP^+ cells (Muller et al., 2007), raising the possibility that SOM^+ cells can also orchestrate disinhibitory effects.

However, because only half the cortical inputs to presumed interneurons targeted CB^+ cells, one or more additional interneuron subtype(s), as yet unidentified, is also involved in the feedforward inhibition mediated by cortical inputs. Given that they do not express CB,

potential candidates include the VIP^+/small CCK^+ cells and the ones expressing 5-HT-3A receptors. Additional experiments will be required to address this question.

Acknowledgments

This work was supported by RO1 grant MH-073610 to DP and NIH Yerkes Center base grant RR-00165 from NCRR.

ROLE OF AUTHORS: All authors had full access to all the data in the study and take responsibility for the integrity of the data and the accuracy of the data analysis. Study concept and design: GU, DP, YS. Acquisition of data: GU, JFP. Analysis and interpretation of data: GU, DP, YS, JFP. Drafting of the manuscript: GU, DP. Critical revision of the manuscript for important intellectual content: YS. Statistical analysis: GU. Obtained funding: DP, YS. Administrative and technical support: JFP. Study supervision: DP, YS.

LITERATURE CITED

Bienvenu TC, Busti D, Magill PJ, Ferraguti F, Capogna M. Cell-type-specific recruitment of amygdala interneurons to hippocampal theta rhythm and noxious stimuli in vivo. Neuron. 2012; 74:1059–1074. [PubMed: 22726836]

Blatow M, Caputi A, Monyer H. Molecular diversity of neocortical GABAergic interneurones. J Physiol. 2005; 562:99–105. [PubMed: 15539393]

Bauer EP, Ledoux JE. Heterosynaptic long-term potentiation of inhibitory interneurons in the lateral amygdala. J Neurosci. 2004; 24:9507–9512. [PubMed: 15509737]

Carlsen J, Heimer L. The basolateral amygdaloid complex as a cortical-like structure. Brain Res. 1988; 441:377–380. [PubMed: 2451985]

Chard PS, Jordan J, Marcuccilli CJ, Miller RJ, Leiden JM, Roos RP, Ghadge GD. Regulation of excitatory transmission at hippocampal synapses by calbindin D28k. Proc Natl Acad Sci USA. 1995; 92:5144–5148. [PubMed: 7761464]

Colonnier, M. The electron-microscopic analysis of the neuronal organization of the cerebral cortex. In: Schmitt, FO.; Worden, FG.; Adelman, G.; Dennis, SG., editors. The organization of the cerebral cortex. MIT Press; Cambridge: 1981. p. 125-152.

DeFelipe J, Fariñas I. The pyramidal neuron of the cerebral cortex: morphological and chemical characteristics of the synaptic inputs. Prog Neurobiol. 1992; 39:563–607. [PubMed: 1410442]

Danober L, Pape H-C. Mechanisms and functional significance of a slow inhibitory potential in neurons of the lateral amygdala. Eur J Neurosci. 1998; 10:853–867. [PubMed: 9753153]

Davis, M. The role of the amygdala in conditioned and unconditioned fear and anxiety. In: Aggleton, JP., editor. The Amygdala: a functional analysis. Oxford University Press; Oxford: 2000. p. 213-287.

Everitt BJ, Cardinal RN, Parkinson JA, Robbins TW. Appetitive behavior: impact of amygdala-dependent mechanisms of emotional learning. Ann N Y Acad Sci. 2003; 985:233–250. [PubMed: 12724162]

Freund TF, Buzsáki G. Interneurons of the hippocampus. Hippocampus. 1996; 6:347–470. [PubMed: 8915675]

Hancock MB. Two color immunoperoxidase staining: visualization of anatomic relationships between immunoreactive neural elements. Am J Anat. 1986; 175:343–352. [PubMed: 2422916]

Hanson PI, Cashikar A. Multivesicular body morphogenesis. Annu Rev Cell Dev Biol. 2002; 28:337–362. [PubMed: 22831642]

Katona IN, Rancz EA, Acsády L, Ledent C, Mackie K, Hájos N, Freund TF. Distribution of CB1 cannabinoid receptors in the amygdala and their role in the control of GABAergic transmission. J Neurosci. 2001; 21:9506–9518. [PubMed: 11717385]

Katsetos CD, Jami MM, Krishna L, Jackson R, Patchefsky AS, Cooper HS. Novel immunohistochemical localization of 28,000 molecular-weight (Mr) calcium binding protein (calbindin-D28k) in enterochromaffin cells of the human appendix and neuroendocrine tumors (carcinoids and small-cell carcinomas) of the midgut and foregut. Arch Pathol Lab Med. 1994; 118:633–639. [PubMed: 8204010]

Kemppainen S, Pitkänen A. Distribution of parvalbumin, calretinin, and calbindin-D28k immunoreactivity in the rat amygdaloid complex and colocalization with gamma-aminobutyric acid. J Comp Neurol. 2000; 426:441–467. [PubMed: 10992249]

Lang EJ, Pare D. Similar inhibitory processes dominate the responses of cat lateral amygdaloid projection neurons to their various afferents. J Neurophysiol. 1997a; 77:341–352. [PubMed: 9120575]

Lang EJ, Pare D. Synaptic and synaptically activated intrinsic conductances underlie inhibitory potentials in cat lateral amygdaloid projection neurons in vivo. J Neurophysiol. 1997b; 77:353–363. [PubMed: 9120576]

Lang EJ, Paré D. Synaptic responsiveness of interneurons of the cat lateral amygdaloid nucleus. Neuroscience. 1998; 83:877–889. [PubMed: 9483571]

LeDoux JE. Emotion circuits in the brain. Annu Rev Neurosci. 2000; 23:155–184. [PubMed: 10845062]

LeDoux JE, Cicchetti P, Xagoraris A, Romanski LM. The lateral amygdaloid nucleus: sensory interface of the amygdala in fear conditioning. J Neurosci. 1990; 10:1062–1069. [PubMed: 2329367]

LeDoux JE, Farb CR, Milner TA. Ultrastructure and synaptic associations of auditory thalamo-amygdala projections in the rat. Exp Brain Res. 1991; 85:577–586. [PubMed: 1717305]

Mahanty NK, Sah P. Calcium-permeable AMPA receptors mediate long-term potentiation in interneurons in the amygdala. Nature. 1998; 394:683–687. [PubMed: 9716132]

Markram H, Toledo-Rodriguez M, Wang Y, Gupta A, Silberberg G, Wu C. Interneurons of the neocortical inhibitory system. Nat Rev Neurosci. 2004; 5:793–807. [PubMed: 15378039]

Martina M, Royer S, Paré D. Cell-type-specific GABA responses and chloride homeostasis in the cortex and amygdala. J Neurophysiol. 2001; 86:2887–2895. [PubMed: 11731545]

Mascagni F, McDonald AJ. Immunohistochemical characterization of cholecystokinin containing neurons in the rat basolateral amygdala. Brain Res. 2003; 976:171–184. [PubMed: 12763251]

Mascagni F, McDonald AJ. A novel subpopulation of 5-HT type 3A receptor subunit immunoreactive interneurons in the rat basolateral amygdala. Neuroscience. 2007; 144:1015–1024. [PubMed: 17150309]

McDonald, AJ. Cell types and intrinsic connections of the amygdala. In: Aggleton, JP., editor. The amygdala: neurobiological aspects of emotion, memory and mental dysfunction. Wiley Liss; New York: 1992. p. 67-96.

McDonald A. Cortical pathways to the mammalian amygdala. Prog Neurobiol. 1998; 55:257–332. [PubMed: 9643556]

McDonald AJ, Augustine JR. Localization of GABA-like immunoreactivity in the monkey amygdala. Neuroscience. 1993; 52:281–294. [PubMed: 8450947]

McDonald AJ, Betette RL. Parvalbumin-containing neurons in the rat basolateral amygdala: morphology and co-localization of Calbindin-D(28k). Neuroscience. 2001; 102:413–425. [PubMed: 11166127]

McDonald AJ, Mascagni F. Colocalization of calcium-binding proteins and GABA in neurons of the rat basolateral amygdala. Neuroscience. 2001; 105:681–693. [PubMed: 11516833]

McDonald AJ, Mascagni F. Immunohistochemical characterization of somatostatin containing interneurons in the rat basolateral amygdala. Brain Res. 2002; 943:237–244. [PubMed: 12101046]

McDonald AJ, Pearson JC. Coexistence of GABA and peptide immunoreactivity in non-pyramidal neurons of the basolateral amygdala. Neurosci Lett. 1989; 100:53–58. [PubMed: 2569703]

McDonald AJ, Muller JF, Mascagni F. GABAergic innervation of alpha type II calcium/calmodulin-dependent protein kinase immunoreactive pyramidal neurons in the rat basolateral amygdala. J Comp Neurol. 2002; 446:199–218. [PubMed: 11932937]

McGaugh JL. Memory: a century of consolidation. Science. 2000; 287:248–251. [PubMed: 10634773]

Muller JF, Mascagni F, McDonald AJ. Synaptic connections of distinct interneuronal subpopulations in the rat basolateral amygdalar nucleus. J Comp Neurol. 2003; 456:217–236. [PubMed: 12528187]

Muller JF, Mascagni F, McDonald AJ. Coupled networks of parvalbumin-immunoreactive interneurons in the rat basolateral amygdala. J Neurosci. 2005; 25:7366–7376. [PubMed: 16093387]

Muller JF, Mascagni F, McDonald AJ. Pyramidal cells of the rat basolateral amygdala: synaptology and innervation by parvalbuminimmunoreactive interneurons. J Comp Neurol. 2006; 494:635–650. [PubMed: 16374802]

Muller JF, Mascagni F, McDonald AJ. Postsynaptic targets of somatostatin-containing interneurons in the rat basolateral amygdala. J Comp Neurol. 2007; 500:513–529. [PubMed: 17120289]

Pape HC, Paré D. Plastic synaptic networks of the amygdala for the acquisition, expression, and extinction of conditioned fear. Physiol Rev. 2010; 90:419–463. [PubMed: 20393190]

Pare D, Smith Y. Distribution of GABA immunoreactivity in the amygdaloid complex of the cat. Neuroscience. 1993; 57:1061–1076. [PubMed: 8309543]

Pare D, Smith Y, Pare J-F. Intra-amygdaloid projections of the basolateral and basomedial nuclei in the cat: Phaseolus vulgarisleucoagglutinin anterograde tracing at the light and electron microscopic level. Neuroscience. 1995; 69:567–583. [PubMed: 8552250]

Paxinos, G.; Watson, C. The rat brain in stereotaxic coordinates. Academic Press; New York: 2007.

Pitkanen A, Amaral DG. Distribution of parvalbumin-immunoreactive cells and fibers in the monkey temporal lobe: the amygdaloid complex. J Comp Neurol. 1993; 331:14–36. [PubMed: 8320347]

Peters A, Palay SL. The morphology of synapses. J Neurocytol. 1996; 25:687–700. [PubMed: 9023718]

Peters, A.; Palay, SL.; Webster, HF. The Fine Structure of the Nervous System. Oxford University Press; New York: 1991.

Pitkänen A, Amaral DG. Distribution of parvalbumin-immunoreactive cells and fibers in the monkey temporal lobe: The amygdaloid complex. J Comp Neurol. 1993; 331:14–36. [PubMed: 8320347]

Rainnie DG, Asprodini EK, Shinnick-Gallagher P. Inhibitory transmission in the basolateral amygdala. J Neurophysiol. 1991; 66:999–1009. [PubMed: 1684384]

Rainnie DG, Mania I, Mascagni F, McDonald AJ. Physiological and morphological characterization of parvalbumin-containing interneurons of the rat basolateral amygdala. J Comp Neurol. 2006; 498:142–161. [PubMed: 16856165]

Russchen FT. Amygdalopetal projections in the cat. I. Cortical afferent connections. A study with retrograde and anterograde tracing techniques. J Comp Neurol. 1982; 206:159–179. [PubMed: 7085926]

Russchen, FT. Cortical and subcortical afferents of the amygdaloid complex. In: Schwarz, R.; Ben-Ari, Y., editors. Excitatory amino acids and epilepsy. Plenum; New York: 1986. p. 35-52.

Shi CJ, Cassell MD. Cortical, thalamic, and amygdaloid projections of rat temporal cortex. J Comp Neurol. 1997; 382:153–175. [PubMed: 9183686]

Shi CJ, Cassell MD. Perirhinal cortex projections to the amygdaloid complex and hippocampal formation in the rat. J Comp Neurol. 1999; 406:299–328. [PubMed: 10102498]

Smith Y, Paré D. Intra-amygdaloid projections of the lateral nucleus in the cat: PHA-L anterograde labeling combined with post-embedding GABA and glutamate immunocytochemistry. J Comp Neurol. 1994; 342:232–248. [PubMed: 7911130]

Smith Y, Pare J-F, Pare D. Cat intraamygdaloid inhibitory network: Ultrastructural organization of parvalbumin-immunoreactive elements. J Comp Neurol. 1998; 391:164–179. [PubMed: 9518267]

Smith Y, Pare JF, Pare D. Differential innervation of parvalbumin-immunoreactive interneurons of the basolateral amygdaloid complex by cortical and intrinsic inputs. J Comp Neurol. 2000; 416:496–508. [PubMed: 10660880]

Somogyi P, Klausberger T. Defined types of cortical interneurone structure space and spike timing in the hippocampus. J Physiol. 2005; 562:9–26. [PubMed: 15539390]

Sorvari H, Soininen H, Paljärvi L, Karkola K, Pitkänen A. Distribution of parvalbumin immunoreactive cells and fibers in the human amygdaloid complex. J Comp Neurol. 1995; 360:185–212. [PubMed: 8522643]

Sosulina L, Graebenitz S, Pape HC. GABAergic interneurons in the mouse lateral amygdala: a classification study. J Neurophysiol. 2010; 104:617–626. [PubMed: 20484532]

Spampanato J, Polepalli J, Sah P. Interneurons in the Basolateral amygdala. Neuropharmacology. 2011; 60:765–773. [PubMed: 21093462]

Szinyei C, Heinbockel T, Montagne J, Pape HC. Putative cortical and thalamic inputs elicit convergent excitation in a population of GABAergic interneurons of the lateral amygdala. J Neurosci. 2000; 20:8909–8915. [PubMed: 11102501]

Turner BH, Herkenham M. Thalamoamygdaloid projections in the rat: A test of the amygdala's role in sensory processing. J Comp Neurol. 1991; 313:295–325. [PubMed: 1765584]

Unal G, Pare J-F, Smith Y, Pare D. Differential connectivity of short- vs. long-range extrinsic and intrinsic cortical inputs to perirhinal neurons. J Comp Neurol. 2013; 521:2538–2550. [PubMed: 23296922]

Washburn MS, Moises HC. Inhibitory responses of rat basolateral amygdaloid neurons recorded in vitro. Neuroscience. 1992; 50:811–830. [PubMed: 1333061]

Witter MP, Groenewegen HJ. Connections of the parahippocampal cortex in the cat. IV. Subcortical efferents. J Comp Neurol. 1986; 252:51–77. [PubMed: 3793975]

Woodruff AR, Sah P. Networks of parvalbumin-positive interneurons in the basolateral amygdala. J. Neurosci. 2007; 27:553–563. [PubMed: 17234587]

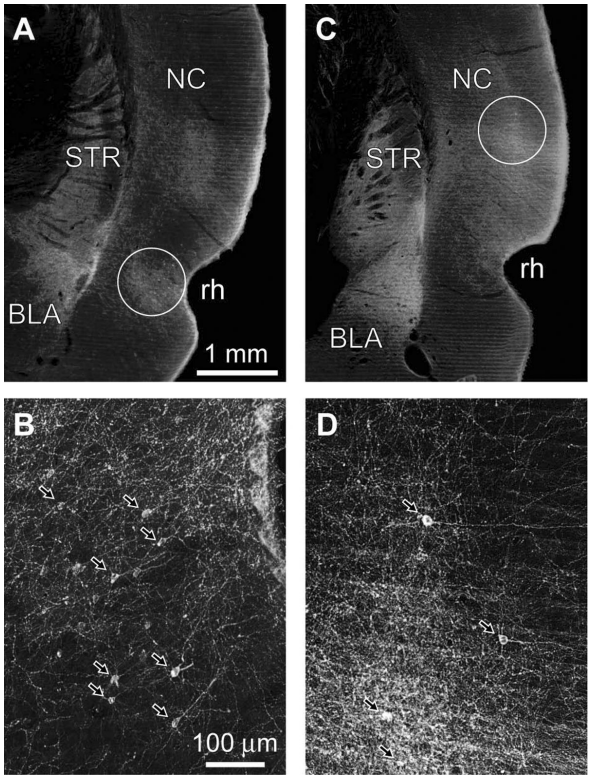

Fig. 1.

Dark-field photomicrographs depicting iontophoretic PHAL injections in the PRC **(A–B)** and NC **(C–D)** at low **(A,C)** and high **(B,D)** magnifications. **(B, D)** Portions of the circled areas in **A** and **C** are depicted at a higher power in **B** and **D**, respectively. Arrows point to PHAL-labeled somata. Scale bars in **A** and **B** apply to **C** and **D**, respectively. BLA, basolateral amygdala; STR, striatum; NC, neocortex; rh, rhinal sulcus.

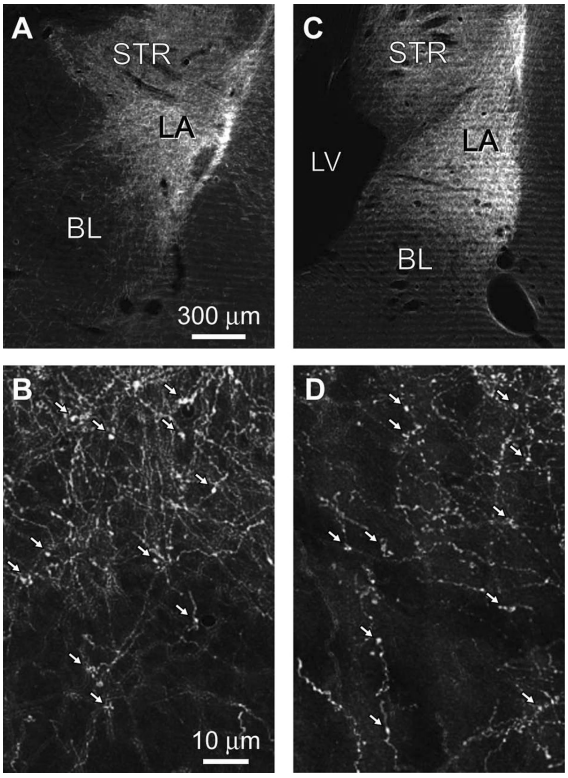

Fig. 2.

PHAL injections in PRC and NC produce anterograde labeling in BLA. Dark-field photomicrographs showing anterogradely-labeled cortical axons in the BLA as a result of the iontophoretic PHAL injections depicted in Fig. 1. Cortical axons arising in PRC (**A–B**) or temporal neocortex (**C–D**) at a low **(A, C)** or high **(B, D)** power. Arrows in **B** and **D** point to PHAL-labeled axonal varicosities. Scales bars in **A** and **B** apply to **C** and **D**, respectively. LA, lateral nucleus; BL, basolateral nucleus; STR, striatum; LV, lateral ventricle.

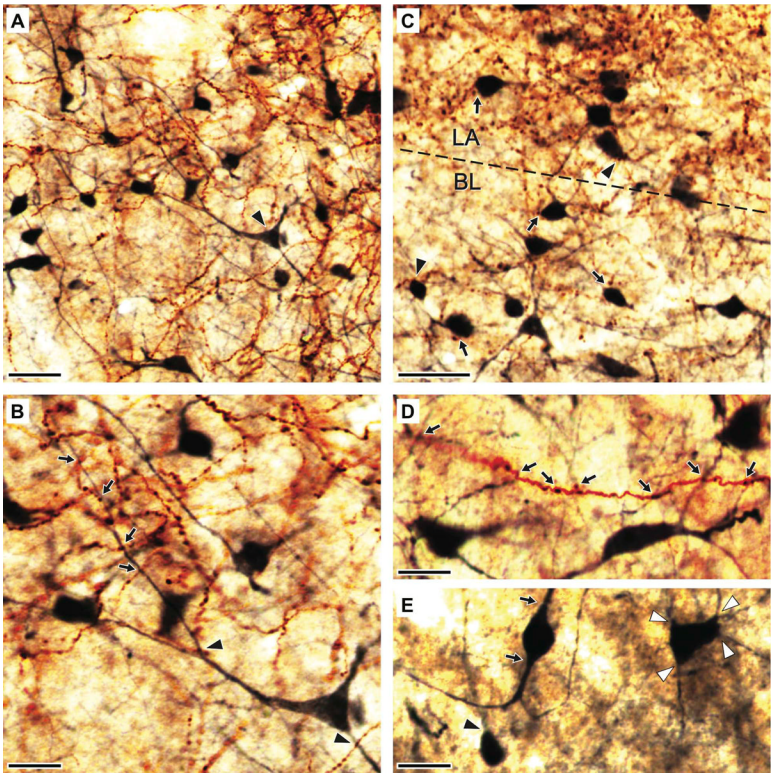

Fig. 3.

Spatial relationship between anterogradely labeled cortical axons and CB+ interneurons of the BLA. (**A**–**E**) Photomicrographs depicting $PHAL^+$ axons (brown reaction product of DAB) and CB-immunoreactive profiles (dark blue reaction product of Ni-DAB) in the BLA. Low- (**A**) and high-power (**B**) images depicting neocortical axons and axonal varicosities and CB^+ somata and dendrites in the ventral portion of LA. The pyramid-shaped multipolar cell marked by an arrowhead in **A** is enlarged in **B** to show its aspiny dendrites. $PHAL^+$ axonal varicosities are seen in close apposition with the proximal (arrowhead) and distal (arrows) dendrites of this neuron. (**C**) A photomicrograph from the LA-BL border (dashed line) depicting spatial relationship between $PHAL^+$ axonal varicosities and CB^+ somata. Typically, a clear gap was seen between $PHAL^+$ boutons and CB^+ somata (arrows). Close appositions (arrowheads) were seen far less frequently. **(D)** Single $PHAL^+$ cortical axon contributing axonal varicosities seen in close apposition with the dendrites of different CB^+ cells (arrows). **(E)** Variations in the shape of CB+ somata. The most common group of cells consisted of multipolar neurons, with four of more dendrites emerging from their somata (white arrowheads). A minority of cells had small, round somata from which emerged a single dendrite (black arrowhead). Also infrequent were neurons with fusiform or ovoid perikarya from which emerged to main dendritic branches (arrows). Scale bars: 40 μm in A; 20 μm in B–E.

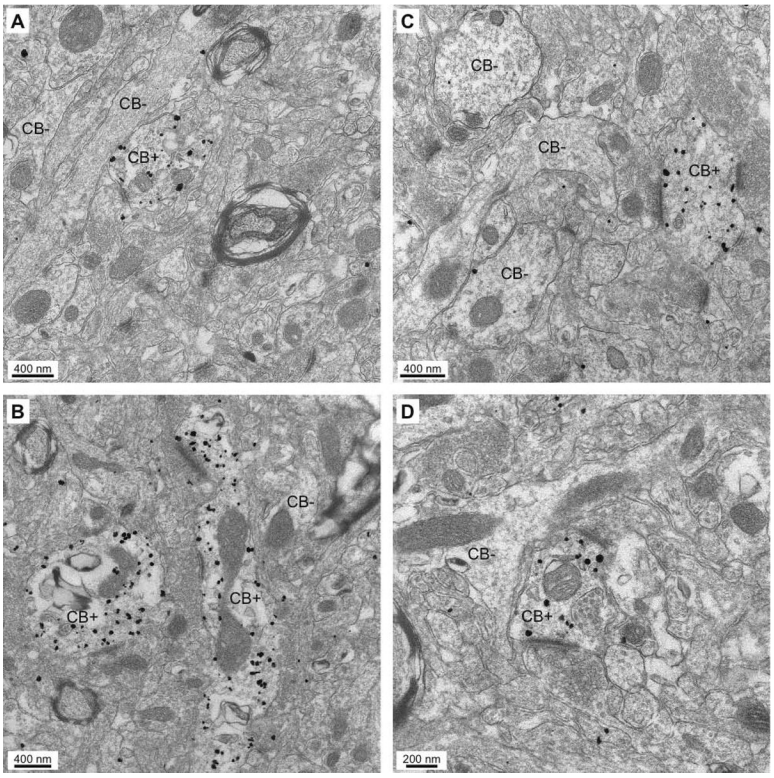

Fig. 4.

Specificity of labeling produced by the pre-embedding immunogold-silver CB immunocytochemistry. **(A–D)** Electron micrographs depicting CB^+ dendritic profiles. They can be easily identified because of the high concentration of gold particles in their confines, with little or no background labeling. Many dendritic profiles in the same electron micrographs are completely devoid of gold particles (CB^-).

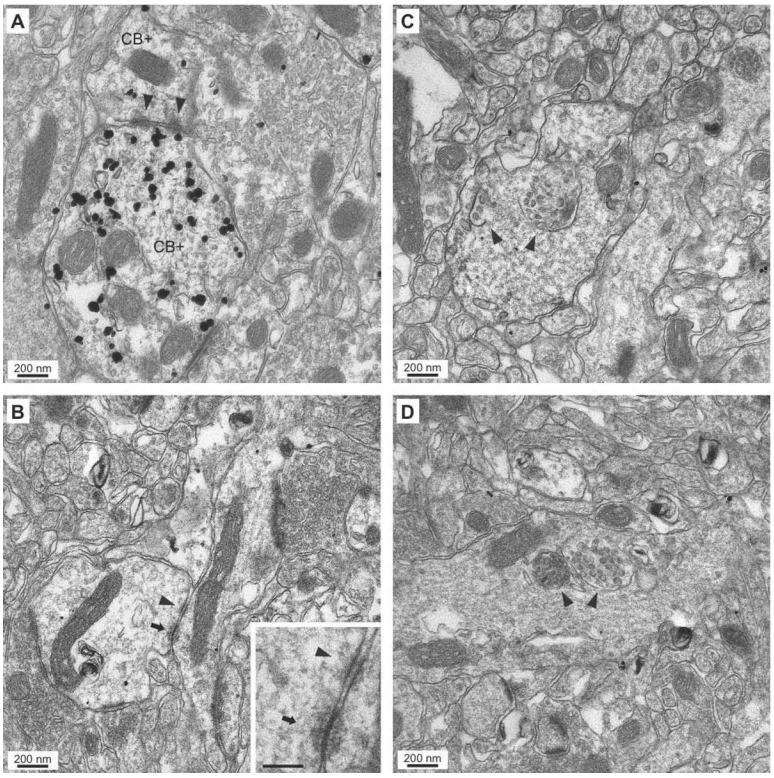

Fig. 5.

Ultrastructural features of CB^+ and CB^- dendritic profiles in the BLA. **(A–B)** Electron micrographs showing dendro-dendritic junctions between CB^+ **(A)** CB^- **(B)** dendrites. **(A)** CB-immunoreactive dendrites (CB+) forming two puncta adhaerentia (arrowheads). **(B)** CB^- dendrites linked via a punctum adhaerens (arrowhead) and a gap junction (arrow). The **inset** shows both junctions at a higher power. Scale bar in inset: 100 nm. **(C–D)** Electron micrographs showing CB^- dendritic profiles containing multivesicular bodies (arrowheads).

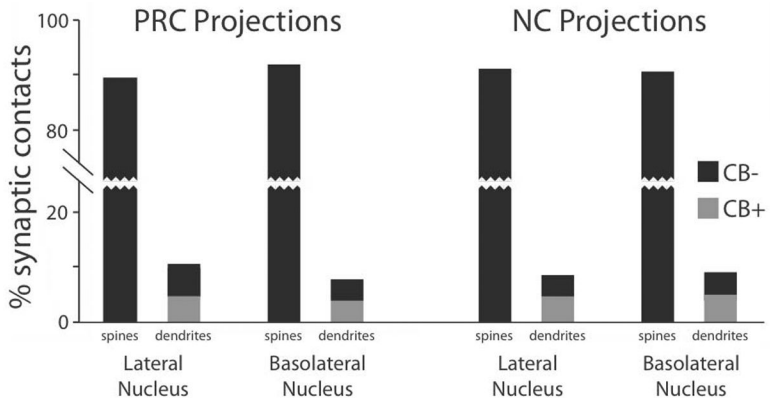

Fig. 6.

Postsynaptic targets of cortical axon terminals in the BLA. Bar graph shows the proportion of $PHAL^{+}$ perirhinal (left-most 4 bars) and temporal neocortical (right-most 4 bars) axon terminals forming asymmetric synapses onto either spines or dendritic profiles (see labels on x-axis). For both injection sites, the left-most and right-most two bars show targets observed in LA or BL, respectively. Black and gray bars indicate CB^{-} and CB^{+} postsynaptic elements, respectively.

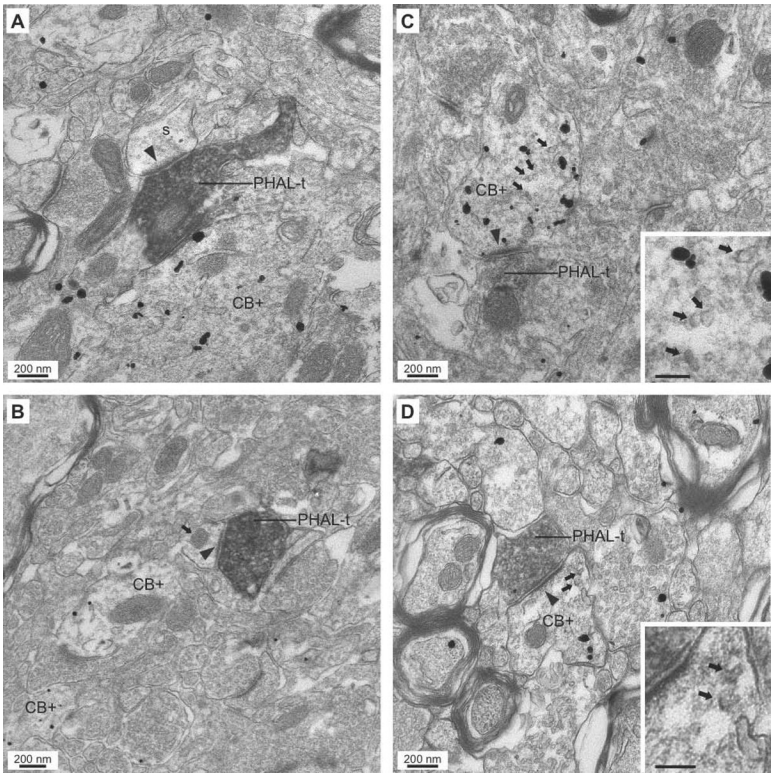

Fig. 7.

Examples of asymmetric synapses (arrowheads) formed by $PHAL^+$ cortical axon terminals (PHAL-t) onto spines **(A)** and dendrites **(B–D)** in the BLA. **(A–B)** Synapses (arrowheads) formed by $PHAL^+$ perirhinal axon terminals with a CB^- spine **(A)** and a CB^- dendrite **(B)** in the presence of a nearby CB^+ dendritic profile. The dendrite in panel B is identified by the presence of a mitochondrion (arrow). **(C–D)** Examples of asymmetric axodendritic synapses (arrowheads) formed by $PHAL^+$ perirhinal **(C)** and neocortical **(D)** axon terminals with CB^+ elements in the BLA. The postsynaptic elements in panels **C** and **D** also represent examples of CB^+ dendrites containing vesicular profiles (arrows). They are depicted at higher power in the insets on the lower right. Scale bars in insets: 100 nm.

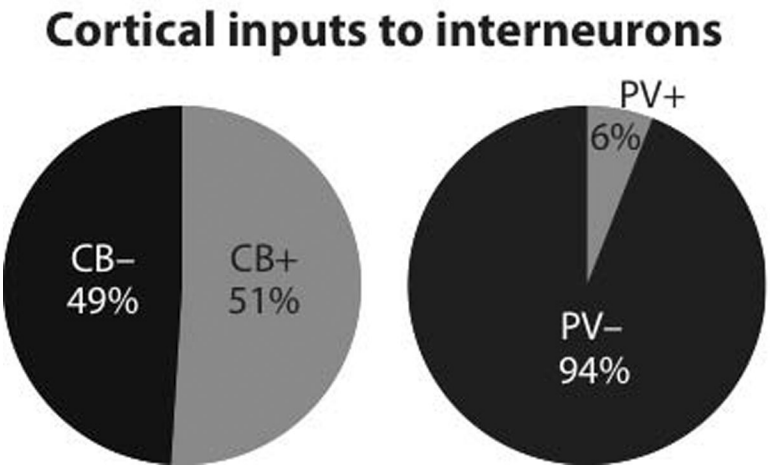

Fig. 8.

Comparison between proportions of cortical synapses onto putative interneurons in material processed to reveal CB immunoreactivity (left, present study) vs. PV immunoreactivity (right, replotted from Smith et al., 2000). A nearly ten-fold higher proportion of $PHAL^{+}$ axons terminals from the cerebral cortex form synapses with CB^{+} profiles than with PV^{+} elements.